López-Fraguas, E., Masi, S., & Mora-Seró, I. (2019). Optical Characterization of Lead-Free Cs2SnI6 Double Perovskite Fabricated from Degraded and Reconstructed CsSnI3 Films. *In ACS Applied Energy Materials, 2*,(12), 8381–8387

DOI: 10.1021/acsaem.9b01827

ACS APPLIED ENERGY MATERIALS
Cite This: ACS Appl. Energy Mater. XXXX, XXX, XXX−XXX
Letter
www.acsaem.org

# Optical Characterization of Lead-Free $Cs_2SnI_6$ Double Perovskite Fabricated from Degraded and Reconstructed $CsSnI_3$ Films

Eduardo López-Fraguas,[†,‡] Sofia Masi,[*,†] and Iván Mora-Seró[*,†]

[†]Institute of Advanced Materials (INAM), Universitat Jaume I, Av. Sos Baynat, s/n, 12071 Castelló, Spain

[‡]Displays and Photonic Applications Group (GDAF-UC3M), Universidad Carlos III de Madrid, Av. Universidad 30, 28911 Leganés (Madrid), Spain

Supporting Information

**ABSTRACT:** Halide perovskites have experienced a huge development in the past years, but they still have two major challenges for their massive implantation: the long-term stability and the use of lead. One of the most obvious lead-free candidates to replace these perovskites is $CsSnI_3$, but due to its poor environmental stability, it has been discarded for the fabrication of stable devices. Nevertheless, ambient degradation of $CsSnI_3$ and ulterior reconstruction produce a relatively stable lead-free $Cs_2SnI_6$ double perovskite with interesting optical properties that have not been deeply characterized previously. In this work, the potential use for the optical properties of $Cs_2SnI_6$ is studied and compared with that of the most common halide perovskite, $CH_3NH_3PbI_3$ ($MAPbI_3$). The $Cs_2SnI_6$ films stayed in a standard atmosphere for a week without showing any signs of degradation. They also demonstrated better reflective behavior than $MAPbI_3$ and higher absorption in the 650 and 730 nm spectral range, making this material interesting for the development of photodetectors in this region. This study demonstrates that $Cs_2SnI_6$ is a promising material for photodevices, as it highlights its main characteristics and optical parameters, giving an original view on the use of the double perovskite, but at the same time emphasizing the need to improve the electrical properties for the development of efficient optoelectronic devices.

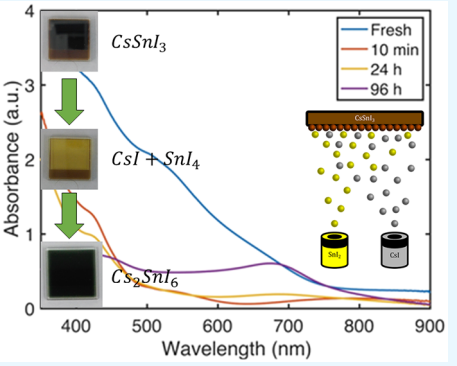


**KEYWORDS:** *optical characterization, lead-free, perovskite, coevaporation deposition, tin halide, full inorganic*

## INTRODUCTION

Lead halide perovskites ($APbX_3$, with A being an organic/inorganic cation and X an halide anion) have experienced a huge development in past years, due to their suitability for the fabrication of solar cells, going from an initial 3.81% power conversion efficiency[1] to the recently achieved 25.2%.[2] These perovskites have demonstrated their great absorption capabilities, high photoluminescence quantum yield, and cheap fabrication processes. All these facts make them great candidates not only for the solar cell world but also for other optoelectronic applications such as solid light emitters[3,4] or as photodetectors.[5−7] However, these systems present a significant drawback facing their commercialization due to the toxicity of the lead. Consequently, a lot of studies focus on the development of lead-free perovskites with characteristics similar to those of their lead counterparts.[8−11]

There are a lot of possible lead-free candidates.[12] However, tin halide perovskites have drawn the attention of the scientific community, due to their similarities with the lead halide perovskites.[13,14] In particular, the fully inorganic $CsSnI_3$ achieved 0.88% efficiency in its first use as a Schottky solar cell.[15] Chung et al. studied the electrical properties of $CsSnI_3$, discussing its metallic behavior instead of a semiconducting one.[16] They argued that this behavior is due to the tin vacancies produced in the structure during its formation.[17−19] Following that, Marshall et al. included a 10% excess of $SnI_2$ in the formation of the film, or 20% of $SnF_2$[20] to cover the tin vacancies, achieving an efficiency around 2−2.76%.[21,22]

The main drawback of this perovskite is the poor stability in environmental conditions, because the $Sn^{2+}$ is easily oxidized to $Sn^{4+}$. Lee et al. tried to avoid this oxidation using $SnF_2$ as a reducing agent in the formation of the formamidinium tin iodide ($FASnI_3$) perovskite, achieving a power conversion efficiency of 4.8%.[23] Recently, Chen et al. mixed the $CsSnI_3$ with germanium (Ge), making a "double perovskite" ($Cs_2SnGeI_6$) with 7.11% efficiency.[24] However, a majority of these studies were carried under a nitrogen atmosphere. Under these conditions, $Sn^{4+}$ arises, transforming $CsSnI_3$ perovskite into $Cs_2SnI_6$ double perovskite. Nevertheless, this material itself constitutes a more air stable candidate than its nonoxidized counterpart.[25] It has been previously used as a hole transport layer (HTL) in dye-sensitized solar cells,[26−28] and also as nanowires[29] or quantum rods.[30] Several synthesis methods have been employed for its preparation.[25,31,32] However, the optical properties of this material have not been broadly studied in the literature. In this work, the optical properties of $Cs_2SnI_6$, obtained as the final

Received: September 17, 2019
Accepted: December 2, 2019
Published: December 2, 2019






DOI: 10.1021/acsaem.9b01827
ACS Appl. Energy Mater. XXXX, XXX, XXX−XXX

degradation product of $CsSnI_3$ in air, are studied in depth. In order to compare the properties of the thin film material and of the bulk, the powder is also synthesized with a novel and easy precipitation method. Moreover, with a comparative analysis of $Cs_2SnI_6$ and of the widely used perovskite, the methylammonium lead iodide ($MAPbI_3$) properties show the potential for $Cs_2SnI_6$ not only in terms of ambient stability but also from the optical point of view. With this study, we intend to pave the way for further electric studies of this promising lead-free material, targeting the fabrication of efficient optoelectronic devices.

## EXPERIMENTAL SECTION

**Thin Film Fabrication.** The $CsSnI_3$ thin film was deposited using a coevaporation technique, as can be schematically seen in Figure 1. We used an MBraun thermal evaporator, filling two crucibles with precursors: one with CsI (99.9%, Sigma-Aldrich) and the other one with $SnI_2$ (99.9%, Sigma-Aldrich). The glass substrates were previously cleaned with a soapy water ultrasonic bath, rinsed with MiliQ water, ultrasonicated with ethanol and isopropanol (1:1), and then ultrasonicated again with ethanol and acetone (1:1).

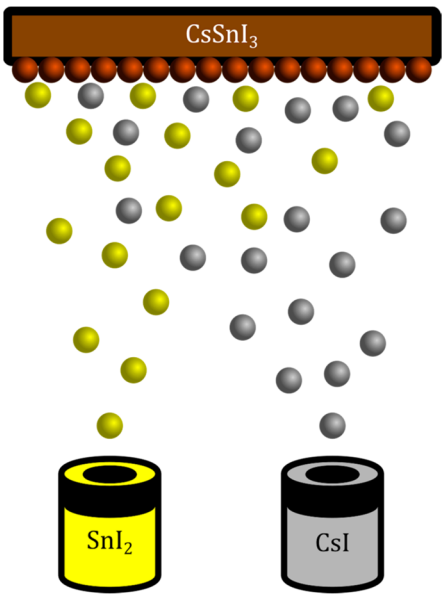


**Figure 1.** Scheme of the thermal coevaporation fabrication process for the preparation of $CsSnI_3$.

The coevaporation of the binary salts leads to the self-assembly of the two precursors and to the formation of the lead-free perovskite (eq 1):

$$1CsI + 1SnI_2 \rightarrow CsSnI_3 \quad (1)$$

The coevaporation process involved heating the two crucibles simultaneously under vacuum, and then sublimation until the desired deposition rate was reached for both precursors.

In order to achieve the correct stoichiometry (1:1) in the final film, it is convenient to calculate the deposition rate ratio. It is, in fact, reasonable that the material volume ratio is proportional to the film thickness, and in turn to the evaporation rate. Thus, the volume ratio, depending on the molecular weight and densities (eq 2), is equal to the rate ratio.

$$\frac{1\ \text{mol CsI}}{1\ \text{mol SnI}_2} \rightarrow \frac{259.81\ \text{g CsI}}{372.52\ \text{g SnI}_2} \rightarrow \frac{57.61\ \text{mL CsI}}{49\ \text{mL SnI}_2} = \frac{\text{deposition rate}_{\text{CsI}}}{\text{deposition rate}_{\text{SnI}_2}} = 1.176 \quad (2)$$

This means that, to achieve the correct stoichiometry, the deposition rate of CsI must be 1.176 times bigger than that of $SnI_2$. With this simple calculation, we can customize the ratio between the two precursors and make films with CsI or $SnI_2$ excess, with different properties.[22,33] The optimized temperature values for each crucible are ~270 °C for $SnI_2$ and ~510 °C for CsI. All these coevaporations took place with the evaporator at $3 \times 10^{-6}$ Torr pressure, inside a nitrogen filled glovebox.

**Reconstruction Conditions.** The conversions to $Cs_2SnI_6$ were carried out in the dark, with a temperature between 21 and 23 °C and relative humidity of 28−35%. The samples were stored in aluminum wrapped boxes in laboratory conditions, in air.

**$Cs_2SnI_6$ Powder Synthesis.** Pure $Cs_2SnI_6$ powder was synthesized with the following procedure. A 1 mmol portion of CsI (259.81 mg) was mixed with 1 mmol of $SnI_2$ (372.52 mg) in a vial. A 1 mL portion of acetone was added to the mixture to form a black suspension, which gently stirred at 750 rpm for a couple of hours, in order to completely disperse the precursors. After the evaporation of the acetone in ambient conditions, it was possible to collect the precipitated black crystals of $Cs_2SnI_6$.

**Materials Characterization.** X-ray diffraction (XRD) measurements of the powders and the thin films were taken by an X-ray diffractometer (D8 Advance, Bruker-AXS) (Cu K$\alpha$, wavelength $\lambda$ = 1.5406 Å). A UV−vis spectrophotometer (Cary 300 UV−vis, Agilent) was used to measure the absorbance, reflectance, and transmittance of the films. Photoluminescence (PL) measurements were done using a spectrofluorometer (Fluorolog, Horiba). The photoluminescence quantum yield (PLQY) measurement was taken using an integrating sphere (Hamamatsu). Thicknesses of the films were obtained using a profilometer (Dektak 6M, Veeco). All of the microscopy was done using a scanning electron microscope (SEM) (JSM-7001F, JEOL) which was also equipped with energy dispersive X-ray spectroscopy (EDS).

## RESULTS AND DISCUSSION

$CsSnI_3$ samples prepared on glass substrates by coevaporation (see Experimental Section) inside the glovebox were characterized under ambient conditions. After 10 min of ambient air exposure, samples experienced a fast degradation to their precursors (Figure 2a) with a decrease of the absorbance (Figure 2b). Accordingly, their color changed from dark brown ($CsSnI_3$, left) to yellow (CsI + $SnI_2$, center). The poor stability of the $CsSnI_3$ in air is mainly due to the decomposition (eq 3) and oxidation (eq 4) mechanisms.

$$CsSnI_3 + \text{environmental conditions} \rightarrow CsI + SnI_2 \quad (3)$$

$$2SnI_2 + O_2 \rightarrow SnI_4 + SnO_2 \quad (4)$$

The oxidation from $Sn^{2+}$ to $Sn^{4+}$ leads to the phase conversion to $Cs_2SnI_6$, in which half of the tin atoms are missed, because they form tin oxide. The complete reaction is shown in eq 5.

$$2CsSnI_3 + O_2 \rightarrow Cs_2SnI_6 + SnO_2 \quad (5)$$

This $CsSnI_3$ degradation and $Cs_2SnI_6$ reconstruction has been demonstrated by Qiu et al.[34] but with some differences. In our case, the degradation and reconstruction take between 3 and 5 days to get the film completely dark (Figure 2a, right) as compared to the 24 h needed in that study. This enhanced stability of initial $CsSnI_3$ is attributed to better quality of the deposition method employed here, as they reported a two-step sequential deposition by alternating thermal evaporation depositions, followed by a thermal annealing to provoke a solid-state reaction between the layers. This method increases the chance of getting pinholes and an inhomogeneous morphology, compared to the film obtained by thermal coevaporation.[34] The absorbance spectra reported in Figure


DOI: 10.1021/acsaem.9b01827
ACS Appl. Energy Mater. XXXX, XXX, XXX−XXX

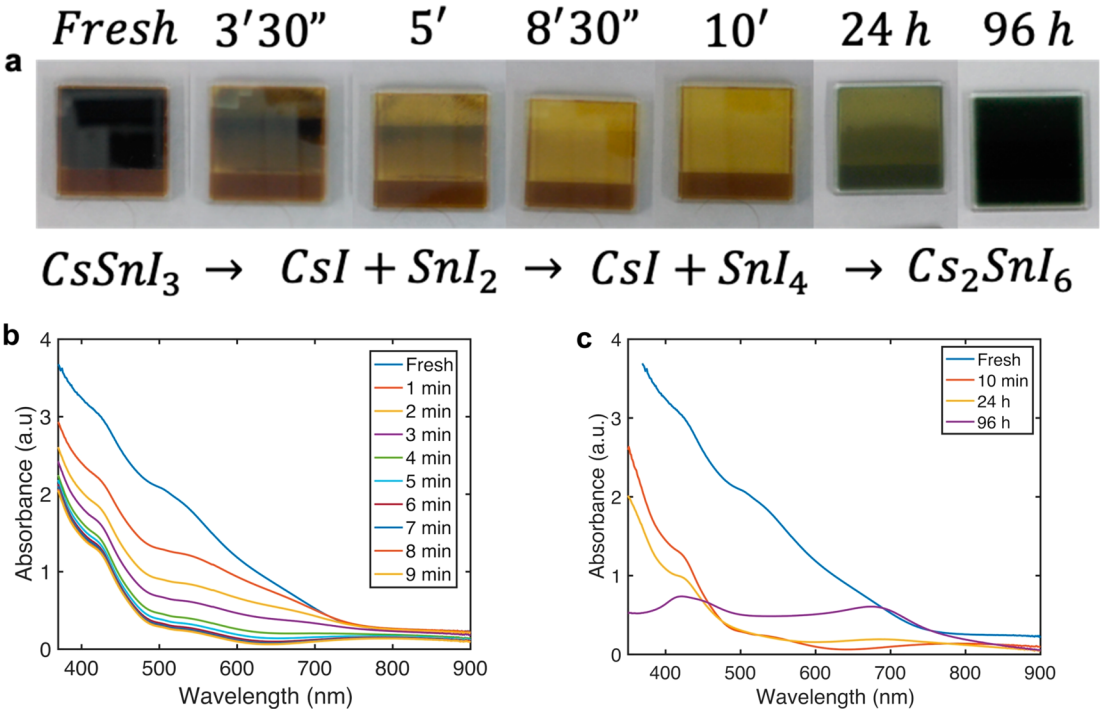


**Figure 2.** (a) Degradation, oxidation of $CsSnI_3$, and reconstruction of the $Cs_2SnI_6$ thin film. (b) Absorbance decay due to $CsSnI_3$ degradation. (c) Absorbance recovery due to formation of $Cs_2SnI_6$.

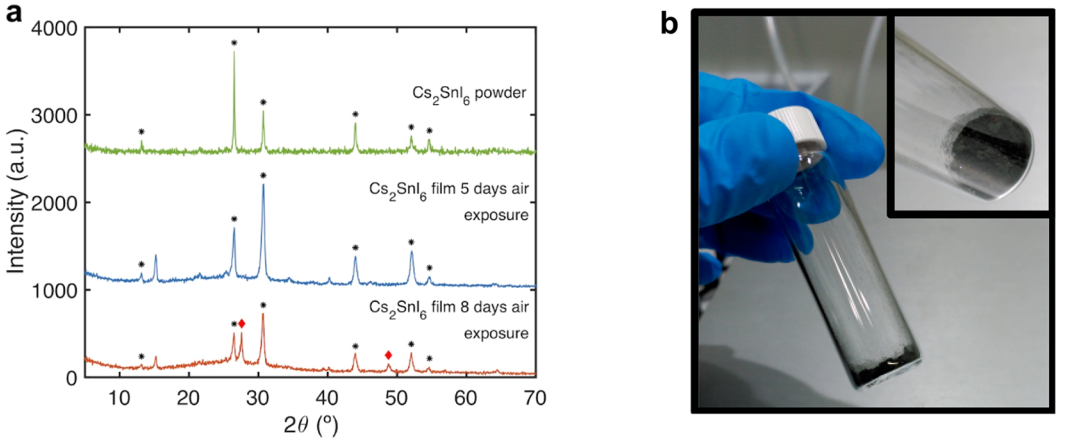


**Figure 3.** (a) XRD patterns of the pure powder and the thin films of $CsSnI_3$ after 5 days and 8 days in air. After the 5th day the $CsSnI_3$ film is totally converted into $Cs_2SnI_6$. Black stars show $Cs_2SnI_6$ peaks, and red diamonds show the CsI peaks. (b) Picture of the $Cs_2SnI_6$ pure powder.

2c show that the film recovers its capacity to absorb the wavelengths between 700 and 800 nm completely, but it loses the absorption capacity in shorter wavelengths and has a planar response with two humps, instead of the original ramp shape. This characteristic behavior, resulting in an average visible transmittance (AVT) of 42.1%, doubling the value of the AVT reported for 150 nm MAPI films,[35,36] is attractive for a semitransparent application.[37] In this case the thickness, measured using a profilometer and by SEM cross section, giving a result of 230 nm (Figure S1a,b), was not sacrificed to obtain a high transmittance value, avoiding the problems related to the contact between the deposited layer above and below the perovskite, leading to a short circuit in optoelectronic devices. Note that slower degradation of $CsSnI_3$ is observed in the inferior side of the analyzed sample, Figure 2a, where FTO (fluorine doped $SnO_2$) is exposed in the substrate. This fact points to a possible effect of fluorine in FTO as a reducing agent[23] in the enhanced stability of $CsSnI_3$ in this region. However, deep analysis of this observation is beyond the scope of this work.

To compare the properties in bulk, we synthesized the $Cs_2SnI_6$ powder following the procedure explained in the Experimental Section. The X-ray diffraction (XRD) patterns of the powder and of the thin film are shown in Figure 3a. Here, we considered the powder (Figure 3b) as a reference pure material, with characteristic peaks at 13.16°, 26.52°, 30.72°, 44°, 52.04°, and 54.68°, all of them representing lattice planes of $Cs_2SnI_6$.[26,32,33] After comparing these peaks with a film exposed to ambient air for 5 days, it is possible to recognize similar patterns in the degraded and reconstructed samples. However, 3 days after this, another two peaks have arisen, at 27.6° and 48.76°, both belonging to CsI, one of the precursors. This fact implies that the films maintain their air stability for 1 week, approximately. Then, they start decomposing into their


DOI: 10.1021/acsaem.9b01827
ACS Appl. Energy Mater. XXXX, XXX, XXX−XXX

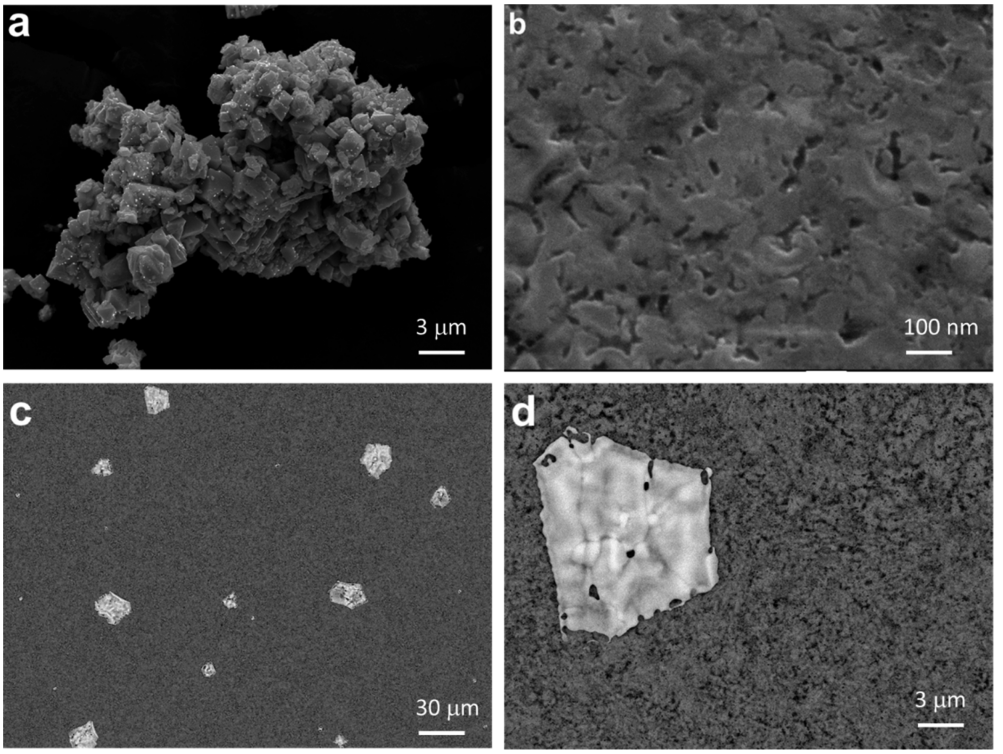


**Figure 4.** Scanning electron microscopy (SEM) images of (a) pure powder sample and (b) $Cs_2SnI_6$ samples. (c) After 11 days on the SEM, the top view of the $Cs_2SnI_6$ CsI crystals became visible. (d) Zoom-in of the CsI crystal detail.

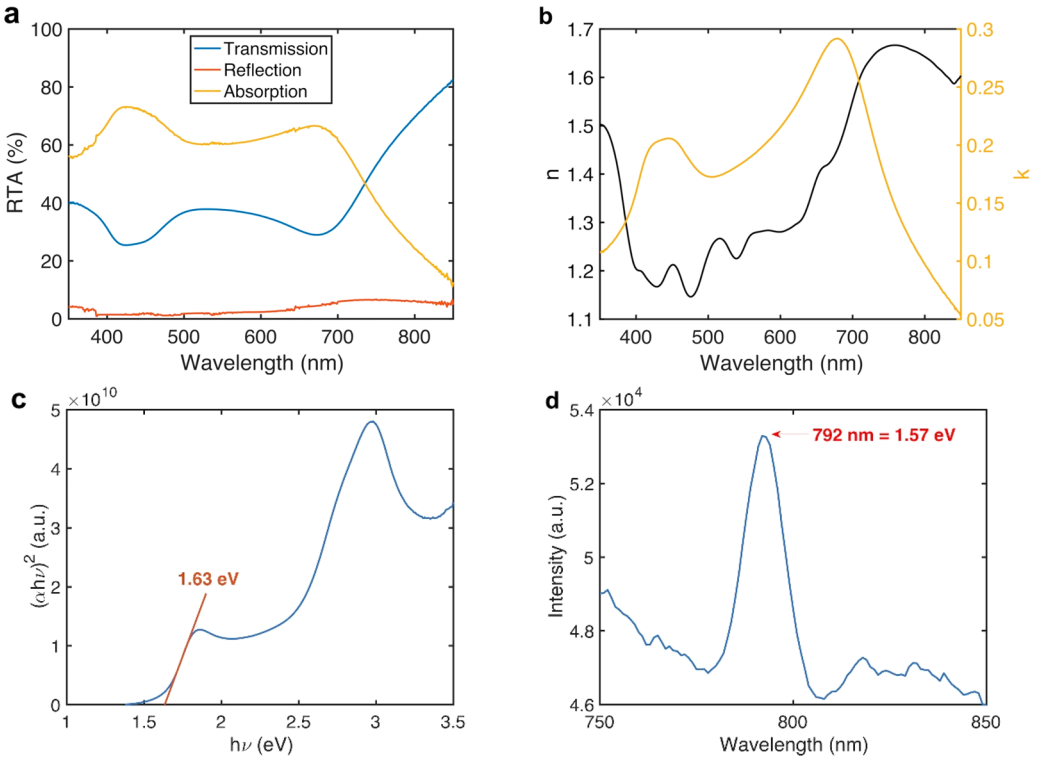


**Figure 5.** Optical characterization of $Cs_2SnI_6$ thin films: (a) reflection, transmission, and absorption measurements; (b) refractive index and extinction coefficient values; (c) Tauc plot determining the band gap; and (d) photoluminescence peak matching with the band gap.

precursors again. This highlights that, despite the $Cs_2SnI_6$ double perovskite presenting an enhanced stability compared with most of its perovskite counterparts, it also requires encapsulation for long-term stability.

To double-check the presence of the CsI, we measured the morphology by scanning electron microscopy (SEM) (Figure 4). The pure powder presents crystals with tiny bright dots in the secondary electron image but not in the backscattered one. In



DOI: 10.1021/acsaem.9b01827
ACS Appl. Energy Mater. XXXX, XXX, XXX−XXX

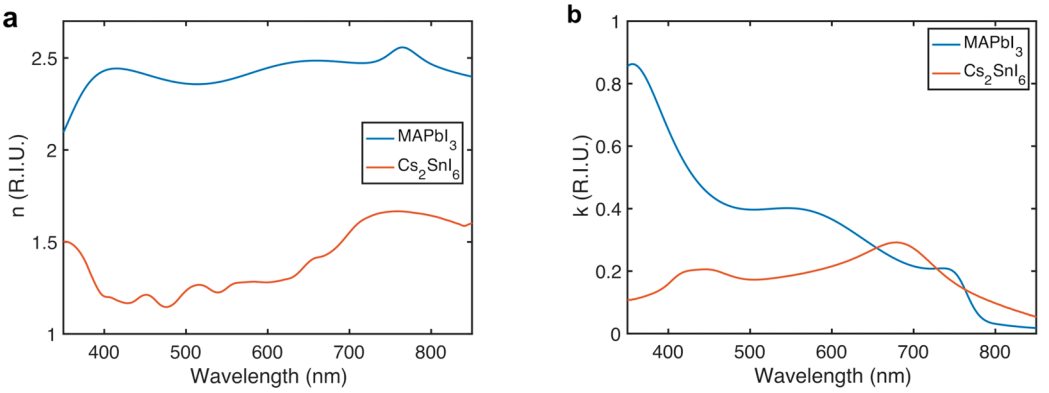


**Figure 6.** (a) Refractive index and (b) extinction coefficient comparison between classical $MAPbI_3$ and lead-free ($Cs_2SnI_6$) perovskite.

fact, the crystal and the bright dots were analyzed using energy-dispersive X-ray spectroscopy (EDS) measurements, with both giving the same result, Cs ≈ 22%, Sn ≈ 11%, and I ≈ 66%, matching the $Cs_2SnI_6$ structure (Figure S2a). Figure 4b shows that the surface of the thin film before the final decomposition is rough. Although it was not possible to measure the $CsSnI_3$ film, because of the fast degradation, we are confident that the morphology is homogeneous, as the coevaporation gives a perfect mirror-like film (Figure S3). Consequently, the roughness observed in $Cs_2SnI_6$ is likely generated during the oxidation and reconstruction process, as briefly mentioned above.

In Figure 4c,d, we can see the surface of the $Cs_2SnI_6$ thin film starting the degradation process, because crystals of CsI start appearing. The composition of the crystals was confirmed by EDS measurements (Figure S2b).

Optical properties of the $Cs_2SnI_6$ thin films prepared by degradation and reconstruction were systematically analyzed. We measured and calculated the absorption coefficient, band gap, refractive index, and extinction coefficient.

The absorption, reflection, and transmission of the films were measured (Figure 5a), and the corresponding values were used to obtain the absorption coefficient, $\alpha$, using the relation below:[38]

$$\alpha = \frac{1}{t}\ln\left[\frac{(1-R)^2}{T}\right] \approx 2.303\frac{A}{t} \tag{6}$$

Here, $t$ is the thickness of the film, and $R$, $T$, and $A$ are reflectance, transmittance, and absorbance of the film, respectively. The approximation showed in eq 6 is accepted if the reflectance is close to zero. In this study, the approximation matches the real case, due to the low reflection of the film (Figure 5a).

The values of refractive index and extinction coefficient as a function of wavelength, see Figure 5b, were obtained following eqs 7 and 8:[38]

$$\kappa = \frac{\alpha\lambda}{4\pi} \tag{7}$$

$$n = \frac{-2(R+1) \pm \sqrt{(2(R+1))^2 - 4(R-1)^2(1+\kappa^2)}}{2(R-1)} \tag{8}$$

In these equations, $\lambda$ is the wavelength, $R$ the measured reflectance, $n$ the refractive index, and $\kappa$ the extinction coefficient.

$Cs_2SnI_6$ thin films presented a band gap of 1.63 eV, see Figure 5c, as it was calculated using the linear interpolation of the Tauc plot. This plot compares $(\alpha h\nu)^n$ ($n = 2$, considering $Cs_2SnI_6$ as a direct band gap material) against the energy of the photons ($h\nu$), where $h$ is Planck's constant and $\nu$ the photon's frequency. Previous literature studies provide a wide range of band gap values for $Cs_2SnI_6$, between 1.2 and 1.6 eV.[25−28,32,34] Our work is in good agreement with studies pointing to a high band gap in this range.[25,27,32,34] Regarding the optical band gap, the photoluminescence (PL) of the thin films results in the emission peak (Figure 5d) at 792 nm. Translated to energy, this value is 1.57 eV, which matches with the result obtained from the Tauc plot, with a relatively small Stokes shift. No significant PL quantum yield was measured for this samples, pointing to a high nonradiative recombination of the material.

In order to put this material in context with other materials of the perovskite family, we compared it with the most studied perovskite, $MAPbI_3$.[39] Figure 6a,b shows the comparison of refractive index and extinction coefficient between both materials. Two main aspects are remarkable here: the first one, regarding $n$, is the huge difference between the $MAPbI_3$ (around 2.5) and the $Cs_2SnI_6$ (around 1.5) values. This fact can make $Cs_2SnI_6$ better than $MAPbI_3$ in terms of reflection and interface index matching, depending on the surrounding layers. The second important fact is regarding $\kappa$, as $MAPbI_3$ can be considered a better absorber than $Cs_2SnI_6$; nevertheless, between 650 and 730 nm, $Cs_2SnI_6$ has a higher extinction coefficient than $MAPbI_3$, which implies that it is a better absorber in this spectral interval. This fact points to a good potential for $Cs_2SnI_6$ for the development of photodetectors in this range.

With these results it is also possible to calculate the ideal short-circuit current density that a solar cell made with $Cs_2SnI_6$ could have. We have done this using the generation rate and by supposing an ideal case with no electrical losses.[40]

$$J_{SC} = q\int_0^T G(x)\,dx$$

$$J_{SC} = q\int_0^T \int_{\lambda_{min}}^{\lambda_{max}} \frac{\lambda}{hc}\mathrm{Irr}(\lambda)[1-r(\lambda)]\alpha(\lambda)\,e^{-\alpha(\lambda)x}\,d\lambda\,dx$$

$$J_{SC} = \frac{q}{hc}\int_{\lambda_{min}}^{\lambda_{max}} \lambda\mathrm{Irr}(\lambda)[1-r(\lambda)](1-e^{-\alpha(\lambda)T})d\lambda$$

In these equations, $q$ is the electron charge, $G(x)$ the generation rate, $h$ Planck's constant, $c$ the speed of light, $\lambda$ the incident wavelength in vacuum, $\alpha$ the absorption coefficient, $T$ the


DOI: 10.1021/acsaem.9b01827
ACS Appl. Energy Mater. XXXX, XXX, XXX−XXX

thickness of the film, $r$ the reflectance, and Irr the irradiance value of the incident light.

Using this equations, under the sun spectrum (AM1.5G), we obtain a $J_{SC}$ value of 18.86 mA/cm$^2$ in a device with an active layer thickness of 230 nm. The maximum value is obtained by supposing ideal conditions (zero reflectance and an optimum optical thickness), and it equals 33.68 mA/cm$^2$. So, making thicker devices will give us higher current density values (e.g., 26.01 mA/cm$^2$ at 500 nm thickness). In thicker cases, several problems start appearing, due to the increase in the distance that the carriers have to travel to reach the electrodes. Nevertheless, these electrical issues are far away from our actual study.

## CONCLUSIONS

In summary, we have prepared a $Cs_2SnI_6$ thin film from the degradation and reconstruction of $CsSnI_3$ first prepared by coevaporation. The structural properties of the $Cs_2SnI_6$ samples were compared with $Cs_2SnI_6$ powders, prepared by a novel method, obtaining a good agreement. $Cs_2SnI_6$ thin films exposed to ambient standard conditions of oxygen and moisture do not exhibit degradation for 1 week. We have successfully characterized the powder and films to obtain their crystalline structure, band gap, morphology, and optical properties (PL, absorption coefficient, band gap, refractive index and extinction coefficient). These values have been compared with $MAPbI_3$ perovskite, revealing that $Cs_2SnI_6$ presents better reflective properties than $MAPbI_3$. In addition, despite $MAPbI_3$ presenting higher absorption than $Cs_2SnI_6$ in most of the visible wavelength range, this is not the case in the spectral range between 650 and 730 nm, where $Cs_2SnI_6$ presents higher light absorption, making this material interesting for the development of photodetectors in this specific range or for semitransparent applications. Further research will be needed to improve the electrical properties of this material limited by high nonradiative recombination as we confirm by PL characterization. All these facts make this lead-free double perovskite, $Cs_2SnI_6$, a great candidate as an absorber for photodevices from an optical point of view and stress the need for further work on the improvement of the electrical properties.

## ASSOCIATED CONTENT

### Supporting Information

The Supporting Information is available free of charge at https://pubs.acs.org/doi/10.1021/acsaem.9b01827.

Scanning electron microscopy cross section, energy-dispersive X-ray spectroscopy results, and pictures of the evaporated films (PDF)

## AUTHOR INFORMATION


### Corresponding Authors

*E-mail: masi@uji.es.

*E-mail: sero@uji.es.

### ORCID

Eduardo López-Fraguas: 0000-0002-7943-4471

Iván Mora-Seró: 0000-0003-2508-0994


### Notes

The authors declare no competing financial interest.

## ACKNOWLEDGMENTS

E.L.-F. wants to express his gratitude to the Ministerio de Educación y Formación Profesional for his doctoral grant (FPU research fellowship FPU17/00612) and his research stay grant (EST18/00399). This work was partially supported by the European Research Council (ERC) via Consolidator Grant (724424-No-LIMIT) and the European Commission via FET Open Grant (862656 - DROP-IT). We acknowledge SCIC from Jaume I University (UJI) for help with XRD and SEM-EDS characterization.

## REFERENCES


(1) Kojima, A.; Teshima, K.; Shirai, Y.; Miyasaka, T. Organometal Halide Perovskites as Visible-Light Sensitizers for Photovoltaic Cells. *J. Am. Chem. Soc.* **2009**, *131*, 6050−6051.

(2) Dissado, L. A.; Nigmatullin, R. R.; Hill, R. M. The Fading of Memory During the Regresion of Structural Fluctuations. *Adv. Chem. Phys.* **2007**, *63*, 253.

(3) Wang, J.; Wang, N.; Jin, Y.; Si, J.; Tan, Z.-K.; Du, H.; Cheng, L.; Dai, X.; Bai, S.; He, H.; Ye, Z.; Lai, M. L.; Friend, R. H.; Huang, W. Interfacial Control Toward Efficient and Low-Voltage Perovskite Light-Emitting Diodes. *Adv. Mater.* **2015**, *27*, 2311−2316.

(4) Fakharuddin, A.; Shabbir, U.; Qiu, W.; Iqbal, T.; Sultan, M.; Heremans, P.; Schmidt-Mende, L. Inorganic and Layered Perovskites for Optoelectronic Devices. *Adv. Mater.* **2019**, *31*, 1807095.

(5) López-Fraguas, E.; Arredondo, B.; Vega-Colado, C.; Pozo, G. d.; Najafi, M.; Martín-Martín, D.; Galagan, Y.; Sánchez-Pena, J. M.; Vergaz, R.; Romero, B. Visible Light Communication System Using an Organic Emitter and a Perovskite Photodetector. *Org. Electron.* **2019**, *73*, 292−298.

(6) Suárez, I.; Hassanabadi, E.; Maulu, A.; Carlino, N.; Maestri, C. A.; Latifi, M.; Bettotti, P.; Mora-Seró, I.; Martínez-Pastor, J. P. Integrated Optical Amplifier−Photodetector on a Wearable Nanocellulose Substrate. *Adv. Opt. Mater.* **2018**, *6*, 1800201.

(7) Miao, J.; Zhang, F. Recent Progress on Highly Sensitive Perovskite Photodetectors. *J. Mater. Chem. C* **2019**, *7*, 1741−1791.

(8) Chatterjee, S.; Pal, A. J. Influence of Metal Substitution on Hybrid Halide Perovskites: Towards Lead-Free Perovskite Solar Cells. *J. Mater. Chem. A* **2018**, *6*, 3793−3823.

(9) Sani, F.; Shafie, S.; Lim, H. N.; Musa, A. O. Advancement on Lead-Free Organic-Inorganic Halide Perovskite Solar Cells: A Review. *Materials* **2018**, *11* (6), 1008.

(10) Wang, X.; Zhang, T.; Lou, Y.; Zhao, Y. All-Inorganic Lead-Free Perovskites for Optoelectronic Applications. *Mater. Chem. Front.* **2019**, *3*, 365−375.

(11) Fu, H. Review of Lead-Free Halide Perovskites as Light-Absorbers for Photovoltaic Applications: From Materials to Solar Cells. *Sol. Energy Mater. Sol. Cells* **2019**, *193*, 107−132.

(12) Travis, W.; Glover, E. N. K.; Bronstein, H.; Scanlon, D. O.; Palgrave, R. G. On the Application of the Tolerance Factor to Inorganic and Hybrid Halide Perovskites: a Revised System. *Chem. Sci.* **2016**, *7*, 4548−4556.

(13) Konstantakou, M.; Stergiopoulos, T. A Critical Review on Tin Halide Perovskite Solar Cells. *J. Mater. Chem. A* **2017**, *5*, 11518−11549.

(14) Shum, K.; Chen, Z.; Qureshi, J.; Yu, C.; Wang, J. J.; Pfenninger, W.; Vockic, N.; Midgley, J.; Kenney, J. T. Synthesis and Characterization of CsSnI3 Thin Films. *Appl. Phys. Lett.* **2010**, *96* (22), 221903.

(15) Chen, Z.; Wang, J. J.; Ren, Y.; Yu, C.; Shum, K. Schottky Solar Cells Based on CsSnI3 Thin-Films. *Appl. Phys. Lett.* **2012**, *101*, 093901.

(16) Chung, I.; Song, J. H.; Im, J.; Androulakis, J.; Malliakas, C. D.; Li, H.; Freeman, A. J.; Kenney, J. T.; Kanatzidis, M. G. CsSnI3: Semiconductor or Metal? High Electrical Conductivity and Strong Near-Infrared Photoluminescence from a Single Material. High Hole Mobility and Phase-Transitions. *J. Am. Chem. Soc.* **2012**, *134*, 8579−87.

(17) Xiao, Z.; Zhou, Y.; Hosono, H.; Kamiya, T. Intrinsic Defects in a Photovoltaic Perovskite Variant Cs2SnI6. *Phys. Chem. Chem. Phys.* **2015**, *17*, 18900−3.

(18) Maughan, A. E.; Ganose, A. M.; Scanlon, D. O.; Neilson, J. R. Perspectives and Design Principles of Vacancy-Ordered Double Perovskite Halide Semiconductors. *Chem. Mater.* **2019**, *31*, 1184−1195.




DOI: 10.1021/acsaem.9b01827
ACS Appl. Energy Mater. XXXX, XXX, XXX−XXX

(19) Bounos, G.; Karnachoriti, M.; Kontos, A. G.; Stoumpos, C. C.; Tsetseris, L.; Kaltzoglou, A.; Guo, X.; Lü, X.; Raptis, Y. S.; Kanatzidis, M. G.; Falaras, P. Defect Perovskites under Pressure: Structural Evolution of $Cs_2SnX_6$ (X = Cl, Br, I). *J. Phys. Chem. C* **2018**, *122* (42), 24004−24013.
(20) Kumar, M. H.; Dharani, S.; Leong, W. L.; Boix, P. P.; Prabhakar, R. R.; Baikie, T.; Shi, C.; Ding, H.; Ramesh, R.; Asta, M.; Graetzel, M.; Mhaisalkar, S. G.; Mathews, N. Lead-Free Halide Perovskite Solar Cells with High Photocurrents Realized Through Vacancy Modulation. *Adv. Mater.* **2014**, *26* (41), 7122−7127.
(21) Koh, T. M.; Krishnamoorthy, T.; Yantara, N.; Shi, C.; Leong, W. L.; Boix, P. P.; Grimsdale, A. C.; Mhaisalkar, S. G.; Mathews, N. Formamidinium Tin-Based Perovskite with Low Eg for Photovoltaic Applications. *J. Mater. Chem. A* **2015**, *3* (29), 14996−15000.
(22) Marshall, K. P.; Walton, R. I.; Hatton, R. A. Tin Perovskite/Fullerene Planar Layer Photovoltaics: Improving the Efficiency and Stability of Lead-Free Devices. *J. Mater. Chem. A* **2015**, *3*, 11631−11640.
(23) Lee, S. J.; Shin, S. S.; Kim, Y. C.; Kim, D.; Ahn, T. K.; Noh, J. H.; Seo, J.; Seok, S. I. Fabrication of Efficient Formamidinium Tin Iodide Perovskite Solar Cells through SnF(2)-Pyrazine Complex. *J. Am. Chem. Soc.* **2016**, *138*, 3974−7.
(24) Chen, M.; Ju, M. G.; Garces, H. F.; Carl, A. D.; Ono, L. K.; Hawash, Z.; Zhang, Y.; Shen, T.; Qi, Y.; Grimm, R. L.; Pacifici, D.; Zeng, X. C.; Zhou, Y.; Padture, N. P. Highly Stable and Efficient All-Inorganic Lead-Free Perovskite Solar Cells with Native-Oxide Passivation. *Nat. Commun.* **2019**, *10* (1), 1−8.
(25) Ke, J. C.-R.; Lewis, D. J.; Walton, A. S.; Spencer, B. F.; O'Brien, P.; Thomas, A. G.; Flavell, W. R. Ambient-Air-Stable Inorganic Cs2SnI6 Double Perovskite Thin Films Via Aerosol-Assisted Chemical Vapour Deposition. *J. Mater. Chem. A* **2018**, *6*, 11205−11214.
(26) Lee, B.; Stoumpos, C. C.; Zhou, N.; Hao, F.; Malliakas, C.; Yeh, C. Y.; Marks, T. J.; Kanatzidis, M. G.; Chang, R. P. Air-Stable Molecular Semiconducting Iodosalts for Solar Cell Applications: Cs2SnI6 as a Hole Conductor. *J. Am. Chem. Soc.* **2014**, *136*, 15379−85.
(27) Shin, H.; Kim, B.-M.; Jang, T.; Kim, K. M.; Roh, D.-H.; Nam, J. S.; Kim, J. S.; Kim, U.-Y.; Lee, B.; Pang, Y.; Kwon, T.-H. Surface State-Mediated Charge Transfer of Cs2SnI6 and Its Application in Dye-Sensitized Solar Cells. *Adv. Energy Mater.* **2019**, *9* (3), 1803243.
(28) Kaltzoglou, A.; Antoniadou, M.; Kontos, A. G.; Stoumpos, C. C.; Perganti, D.; Siranidi, E.; Raptis, V.; Trohidou, K.; Psycharis, V.; Kanatzidis, M. G.; Falaras, P. Optical-Vibrational Properties of the Cs2SnX6 (X = Cl, Br, I) Defect Perovskites and Hole-Transport Efficiency in Dye-Sensitized Solar Cells. *J. Phys. Chem. C* **2016**, *120*, 11777−11785.
(29) Chen, J.; Luo, Z.; Fu, Y.; Wang, X.; Czech, K. J.; Shen, S.; Guo, L.; Wright, J. C.; Pan, A.; Jin, S. Tin(IV)-Tolerant Vapor-Phase Growth and Photophysical Properties of Aligned Cesium Tin Halide Perovskite (CsSnX3; X = Br, I) Nanowires. *ACS Energy Lett.* **2019**, *4*, 1045−1052.
(30) Chen, L. J.; Lee, C. R.; Chuang, Y. J.; Wu, Z. H.; Chen, C. Synthesis and Optical Properties of Lead-Free Cesium Tin Halide Perovskite Quantum Rods with High-Performance Solar Cell Application. *J. Phys. Chem. Lett.* **2016**, *7*, 5028−5035.
(31) Guo, F.; Lu, Z.; Mohanty, D.; Wang, T.; Bhat, I. B.; Zhang, S.; Shi, S.; Washington, M. A.; Wang, G.-C.; Lu, T.-M. A Two-Step Dry Process for Cs2SnI6 Perovskite Thin Film. *Mater. Res. Lett.* **2017**, *5*, 540−546.
(32) Saparov, B.; Sun, J.-P.; Meng, W.; Xiao, Z.; Duan, H.-S.; Gunawan, O.; Shin, D.; Hill, I. G.; Yan, Y.; Mitzi, D. B. Thin-Film Deposition and Characterization of a Sn-Deficient Perovskite Derivative Cs2SnI6. *Chem. Mater.* **2016**, *28*, 2315−2322.
(33) Song, T.-B.; Yokoyama, T.; Aramaki, S.; Kanatzidis, M. G. Performance Enhancement of Lead-Free Tin-Based Perovskite Solar Cells with Reducing Atmosphere-Assisted Dispersible Additive. *ACS Energy Lett.* **2017**, *2*, 897−903.
(34) Qiu, X.; Cao, B.; Yuan, S.; Chen, X.; Qiu, Z.; Jiang, Y.; Ye, Q.; Wang, H.; Zeng, H.; Liu, J.; Kanatzidis, M. G. From Unstable CsSnI3 to Air-Stable Cs2SnI6: A Lead-Free Perovskite Solar Cell Light Absorber with Bandgap of 1.48 eV and High Absorption Coefficient. *Sol. Energy Mater. Sol. Cells* **2017**, *159*, 227−234.
(35) Della Gaspera, E.; Peng, Y.; Hou, Q.; Spiccia, L.; Bach, U.; Jasieniak, J. J.; Cheng, Y.-B. Ultra-Thin High Efficiency Semi-transparent Perovskite Solar Cells. *Nano Energy* **2015**, *13*, 249−257.
(36) Masi, S.; Rizzo, A.; Munir, R.; Listorti, A.; Giuri, A.; Esposito Corcione, C.; Treat, N. D.; Gigli, G.; Amassian, A.; Stingelin, N.; Colella, S. Organic Gelators as Growth Control Agents for Stable and Reproducible Hybrid Perovskite-Based Solar Cells. *Adv. Energy Mater.* **2017**, *7*, 1602600.
(37) Eperon, G. E.; Burlakov, V. M.; Goriely, A.; Snaith, H. J. Neutral Color Semitransparent Microstructured Perovskite Solar Cells. *ACS Nano* **2014**, *8*, 591−598.
(38) Hecht, E.; Zając, A. *Optics*; Addison-Wesley Pub. Co., 1974.
(39) Phillips, L. J.; Rashed, A. M.; Treharne, R. E.; Kay, J.; Yates, P.; Mitrovic, I. Z.; Weerakkody, A.; Hall, S.; Durose, K. Dispersion Relation Data for Methylammonium Lead Triiodide Perovskite Deposited on a (100) Silicon Wafer Using a Two-Step Vapour-Phase Reaction Process. *Data in Brief* **2015**, *5*, 926−928.
(40) Luque, A.; Hegedus, S. *Handbook of Photovoltaic Science and Engineering*; Wiley, 2003.


DOI: 10.1021/acsaem.9b01827
*ACS Appl. Energy Mater.* XXXX, XXX, XXX−XXX